

International Journal of Modern Physics A  
 © World Scientific Publishing Company

## Cronin effect and high $p_{\perp}$ suppression from Color Glass Condensate\*

KAZUNORI ITAKURA†

*Service de Physique Théorique, CEA/Saclay, F-91191, Gif-sur-Yvette, France*

We present an analytical understanding of properties of the ratio between gluon distributions of a nucleus and a proton based on the framework of the Color Glass Condensate. This ratio is closely related to the nuclear modification factor in the deuteron-Au collisions measured by Brahms experiment at RHIC.

### 1. Motivation – The Brahms data in deuteron-Au collisions

The Color Glass Condensate has recently come under the spotlight with the experimental results<sup>1</sup> for the nuclear modification factor in the deuteron-Au collisions measured by the Brahms experiment at RHIC. This is because the global behaviour of the experimental data was qualitatively consistent with the predictions made by the Color Glass Condensate.<sup>2,3</sup> However, the detailed mechanism behind the phenomena was not clear at that time, and we have made a detailed analysis based on analytical calculations.<sup>4</sup> In this talk, I present a summary of our results.

Let me first explain the main results of the Brahms experiment. The nuclear modification factor is a function of transverse momentum  $p_{\perp}$  and rapidity  $y$  of the produced hadrons and is defined by

$$R_{dAu}(p_{\perp}, y) = \frac{\frac{dN_{dAu}}{d^2pdy}}{N_{\text{coll}} \frac{dN_{pp}}{d^2pdy}} \quad (1)$$

where  $dN_{dAu}/d^2pdy$  and  $dN_{pp}/d^2pdy$  are multiplicities of hadrons per unit of phase space in dAu and pp collisions. This quantity is normalized so that  $R_{dAu} = 1$  corresponds to the "null effect", namely, when the dAu collision is simply a collection of pp collisions, which is expected to be realized at very high transverse momentum. Therefore, any deviation from 1 indicates something collective which is not seen in the pp collisions. The Brahms experiment plotted this ratio as a function of transverse momentum  $p_{\perp}$  at different values of rapidity  $y$  (for simplicity, we do not distinguish between rapidity and pseudo-rapidity). The data show the following properties:

\*Based on the collaboration with Edmond Iancu and Dionysis Triantafyllopoulos.

†e-mail: itakura@spht.saclay.cea.fr

2 *Kazunori Itakura*

1. At mid-rapidity  $y = 0$ , the ratio  $R_{dAu}$  becomes larger than 1 for  $p_{\perp} > 2$  GeV, and appears to be saturated for higher momentum  $p_{\perp} \sim 5$  GeV. Since the ratio must go to 1 at extremely high  $p_{\perp}$ , it is natural to say that there is a peak. This is called the Cronin peak.
2. As the rapidity is increased, the magnitude of the ratio  $R_{dAu}$  gets suppressed and becomes smaller than 1 for all the measured transverse momentum  $p_{\perp} < 4$  GeV. Besides, the shape of  $R_{dAu}$  looks flat<sup>a</sup> at high  $p_{\perp}$  and the peak structure seems to disappear.
3. The ratio  $R_{CP}(p_{\perp}, y)$  of the central to peripheral collisions is also measured and the data show that, at mid-rapidity  $y = 0$ , more central collisions give larger Cronin effect, while at forward rapidity  $y = 3.2$ , more central leads to more suppression.

In order to have an analytic understanding of these phenomena, we consider the ratio between the gluon distributions in a nucleus and a proton:

$$\mathcal{R}_{pA}(p_{\perp}, y) \equiv \frac{\varphi_A(p_{\perp}, y)}{A^{1/3} \varphi_p(p_{\perp}, y)}. \quad (2)$$

This quantity is closely related to the nuclear modification factor (1). This is reasonable because, within the  $k_{\perp}$  factorization formula, the difference between multiplicities of pA and pp collisions comes only from the gluon distributions of the targets. In fact, the qualitative equivalence of the two quantities is numerically checked.<sup>3</sup> In other words, the ratio (2) is a more fundamental quantity which directly measures nuclear collective effects, and the properties of the ratio (2) are transferred into those of the nuclear modification factor (1). Therefore, one can analytically understand the physics behind the Brahm's data by investigating the ratio (2).

## 2. Cronin effect at lower energies

We assume that one can use the McLerran-Venugopalan (MV) model to study the Cronin effect at lower rapidities, which corresponds to not-so-high energies. This model is applicable because it is essentially equivalent to the multiple collisions of the Glauber type, and because one can ignore the effect of quantum evolution.

The nuclear gluon distribution from the MV model with a fixed coupling reads

$$\varphi_A(p_{\perp}) = \int d^2 r_{\perp} e^{-ip_{\perp} \cdot r_{\perp}} \frac{1 - \exp\left\{-\frac{1}{4} r_{\perp}^2 Q_A^2 \ln \frac{4}{r_{\perp}^2 \Lambda^2}\right\}}{\pi \alpha_s N_c r_{\perp}^2}, \quad (3)$$

where  $\Lambda$  is a non-perturbative scale of order  $\Lambda_{\text{QCD}}$ ,  $N_c = 3$ , and  $Q_A^2 = \alpha_s N_c \mu_A \propto A^{1/3}$  is proportional to the color charge squared  $\mu_A$  of the valence quarks per unit transverse area. The saturation scale can be defined by the transverse scale when the exponent of the integrand above is of the order of 1. This yields

$$Q_s^2(A) = \alpha_s N_c \mu_A \ln \frac{Q_s^2(A)}{\Lambda^2} \sim A^{1/3} \ln A^{1/3}. \quad (4)$$

<sup>a</sup>The experimental data at forward rapidity  $y = 3.2$  have been updated and now show rather a flat behaviour at high momentum. See the version 2 of Ref. 1.

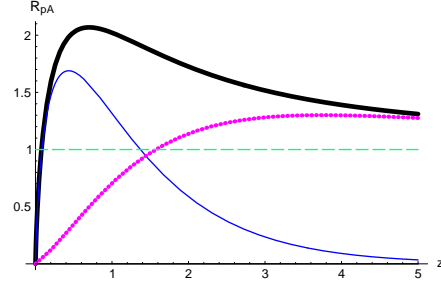


Fig. 1.  $\mathcal{R}_{pA}$  as a function of the scaled momentum variable  $z = p_\perp^2/Q_s^2(A)$  from the MV model with fixed coupling. The thick solid line corresponds to the ratio  $\mathcal{R}_{pA}$ , while the thin solid line and dotted line are the saturation and twist contributions, respectively.

The saturation scale separates the linear and non-linear regimes. At high transverse momentum  $p_\perp \gg Q_s(A)$  which corresponds to the linear regime, the distribution (3) gives the Bremsstrahlung spectrum:

$$\varphi_A(p_\perp) \simeq \frac{\mu_A}{p_\perp}, \quad \text{for } p_\perp \gg Q_s(A), \quad (5)$$

which means that at this transverse momentum, the nucleus looks simply a collection of perturbative nucleons  $\mu_A = A^{1/3}\mu_p$ , and thus  $\varphi_A \simeq A^{1/3}\varphi_p$ . On the other hand, at low transverse momenta  $p_\perp \ll Q_s(A)$ , the gluon distribution is given by

$$\varphi_A(p_\perp) \simeq \frac{1}{\alpha_s N_c} \left\{ \ln \frac{Q_s^2(A)}{p_\perp^2} + \mathcal{O}(1) \right\}, \quad \text{for } p_\perp \ll Q_s(A). \quad (6)$$

Note the overall factor  $1/\alpha_s$  which becomes large for the weak coupling  $\alpha_s \ll 1$ .

One can separate the whole integral in eq. (3) into "saturation" and "twist" contributions  $\varphi_A = \varphi_A^{sat} + \varphi_A^{twist}$ . The twist contribution is a part which can be expanded in powers of  $Q_s^2(A)/p_\perp^2$ , and contains the Bremsstrahlung spectrum (5) as the leading contribution. This twist contribution becomes less and less important as the momentum becomes small. On the other hand, the saturation part  $\varphi_A^{sat}$  remains large at small momentum  $p_\perp < Q_s(A)$  and is explicitly given by  $\varphi_A^{sat}(z) = \frac{1}{\alpha_s N_c} \Gamma(0, z)$ , with  $z = p_\perp^2/Q_s^2(A)$ . At small  $z$ , this reproduces eq. (6).

If one takes the Bremsstrahlung spectrum for the proton distribution  $\varphi_p$  (this is reasonable because the saturation scale of a proton is very small at lower energies and thus the proton is in the linear regime for the kinematical regime of our interest), the change of behaviour of the nuclear gluon distribution mentioned above leads to a nontrivial shape of the ratio  $\mathcal{R}_{pA}$ :

$$\begin{aligned} \mathcal{R}_{pA} &\ll 1 & p_\perp &\ll Q_s(A) \\ \mathcal{R}_{pA} &\sim \ln A^{1/3} > 1 & p_\perp &\sim Q_s(A) \\ \mathcal{R}_{pA} &\rightarrow 1^+ & p_\perp &\gg Q_s(A). \end{aligned} \quad (7)$$

In Fig. 1, we have shown the full contribution as well as the saturation and twist contributions  $\mathcal{R}_{pA}^{sat/twist} = \varphi_A^{sat/twist}/\varphi_A^{BS}$  where  $\varphi_A^{BS} = A^{1/3}\varphi_p = \mu_A^2/p_\perp^2$ . Obviously,

4 Kazunori Itakura

the ratio develops a pronounced peak around the saturation scale. The location and height of the Cronin peak are essentially determined by the saturation contribution, and can be computed analytically in an expansion in powers of  $1/\ln[Q_s^2(A)/\Lambda^2]$ . The leading order results are  $z_{max} \simeq 0.435$ ,  $\mathcal{R}_{pA}(z_{max}) \simeq 0.281 \ln[Q_s^2(A)/\Lambda^2]$ . Note that the height of the Cronin peak  $\mathcal{R}_{pA}(z_{max})$  is enhanced for larger  $A$ . This is consistent with the behaviour of  $R_{CP}$  at mid-rapidity, since the peripheral collision can be regarded as the collision of the nucleus with smaller  $A$ .

### 3. High $p_\perp$ suppression at large energies

Moving to forward rapidities corresponds to seeing smaller  $x$  contribution of the target. In order to describe the gluon distribution at higher energies, one has to include the effects of quantum evolution with respect to  $y = \ln 1/x$  into the MV model which was used for the gluon distribution at lower energy. This can be done by solving the Balitsky-Kovchegov equation with the MV model as the initial condition. Then, one finds three kinematical regimes where the gluon distribution shows qualitatively different behaviours. These are the **CGC** regime  $p_\perp \ll Q_s(A, y)$ , in which the gluons are deeply saturated, the **BFKL** regime  $Q_s(A, y) \ll p_\perp \ll Q_g(A, y)$ , in which the geometric scaling approximately holds while the evolution is described by the linear BFKL equation, and the **DLA** (double log approximation) regime  $p_\perp \gg Q_g(A, y)$ , in which the effect of saturation is totally ignored. Note that the saturation scale which separates the CGC and BFKL regimes is now energy (rapidity) dependent:

$$Q_s^2(A, y) = Q_s^2(A) e^{c\bar{\alpha}_s y}, \quad (8)$$

where  $c \simeq 4.88$  and  $\bar{\alpha}_s = \alpha_s N_c / \pi$ . The scale  $Q_g(A, y)$  which separates the BFKL and DLA regimes is given by

$$Q_g^2(A, y) \simeq Q_s^4(A, y) / Q_s^2(A). \quad (9)$$

More precisely, this scale gives the upper limit of the geometric scaling<sup>5</sup> and has nothing to do with the DLA regime. However, since, in the fixed coupling case, the upper kinematical limit for the BFKL equation happens to roughly coincide with  $Q_g(A, y)$ , one can practically use  $Q_g(A, y)$  as the separation scale for the BFKL and DLA regimes. The same thing does not occur in the running coupling case.

In each regime, the gluon distribution of a nucleus is approximately given by

$$\varphi_A(p_\perp, y) \simeq \frac{1}{\alpha_s N_c} \ln \frac{Q_s^2(A, y)}{p_\perp^2}, \quad \text{if } p_\perp \in \text{CGC} \quad (10)$$

$$\varphi_A(p_\perp, y) \simeq \frac{1}{\alpha_s N_c} \left( \frac{Q_s^2(A, y)}{p_\perp^2} \right)^\gamma \left\{ \ln \frac{p_\perp^2}{Q_s^2(A, y)} + \Delta \right\}, \quad \text{if } p_\perp \in \text{BFKL} \quad (11)$$

$$\varphi_A(p_\perp, y) \simeq \frac{\mu_A}{p_\perp^2} \exp \left\{ \sqrt{4\bar{\alpha}_s y \ln[p_\perp^2 / Q_s^2(A)]} \right\}, \quad \text{if } p_\perp \in \text{DLA} \quad (12)$$

where  $\gamma \simeq 0.63$  and  $\Delta$  is some undetermined constant of the order of 1. The difference  $1-\gamma \simeq 0.37$  is called the anomalous dimension. Note that the gluon distribution

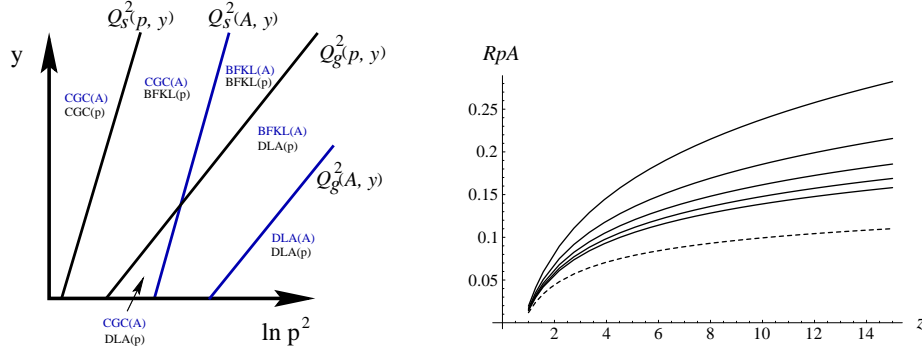


Fig. 2. **Left:** Evolution map for the proton and nucleus. **Right:**  $\mathcal{R}_{pA}$  in the double BFKL regime as a function of  $z = p_{\perp}^2 / Q_s^2(A, y)$ . The solid lines correspond to  $y = 0.75 + 0.3n$ , with  $n = 0, \dots, 4$  from top to bottom. The dashed line is the asymptotic ( $y \rightarrow \infty$ ) profile.

in the CGC and BFKL regimes is a function of  $Q_s^2(A, y) / p_{\perp}^2$ : This is the geometric scaling. The same property cannot be seen in the DLA regime. One can obtain the gluon distribution for the proton target by putting  $A = 1$ .

Since we have three different regimes for both the nucleus and the proton, and the saturation scale of the nucleus is much larger than that of the proton by a factor of  $A^{1/3}$ :  $Q_s^2(A, y) = A^{1/3} Q_s^2(p, y)$ , one has to treat totally six different kinematical regimes as is indicated in Fig. 2 (left). However, since we know the analytic expression of the gluon distribution in each regime, it is now easy to form the ratio  $\mathcal{R}_{pA}$ . To see the behaviour of the ratio  $\mathcal{R}_{pA}$  at high momentum, let us consider the "double BFKL regime" where both the nucleus and proton are in the BFKL regime described by eq. (11). The result is shown in Fig. 2 (right). As the rapidity is increased, the ratio is more and more suppressed. For all the rapidities considered here, the ratio is a monotonically increasing function of  $z = p_{\perp}^2 / Q_s^2(A, y)$ . This global behaviour is consistent with the Brahm's data at forward rapidity.

Physically, the suppression of the ratio  $\mathcal{R}_{pA}$  is induced by the mismatch between the evolution speeds of the nucleus and proton. For the same (large) transverse momentum, the nucleus is always closer to saturation than the proton. The proton has more phase space to evolve and  $\varphi_p$  in the denominator of the ratio grows faster, while the nucleus evolves only slowly. Therefore, in effect, the ratio is suppressed as the energy is increased.

One can also prove that the ratio is a decreasing function of  $A$ , which is consistent with the experimental results for  $R_{CP}$  at forward rapidity.

#### 4. Effects of running coupling

As we go to higher rapidities, the effects of a running coupling becomes important. Here we discuss how the previous results are modified if one includes the effects of a running coupling  $\alpha_s(Q^2) \equiv b_0 / \ln(Q^2 / \Lambda_{\text{QCD}}^2)$ .

Since the MV model is a classical approximation, eq. (3) is a priori written for

6 *Kazunori Itakura*

a fixed coupling  $\alpha_s$ . However, to be consistent with the running coupling evolution, we need to define the running coupling version of the MV model. Formally, this is obtained from eq. (3) by replacing  $\alpha_s \rightarrow \alpha_s(4/r_\perp^2)$  within the denominator of the integrand, and also within  $Q_A^2$ :

$$\varphi_A(p_\perp) = \int d^2 r_\perp e^{-i p_\perp \cdot r_\perp} \frac{1 - e^{-\frac{1}{4} r_\perp^2 Q_A^2}}{\pi b_0 N_c r_\perp^2} \ln \frac{4}{r_\perp^2 \Lambda^2}, \quad (13)$$

where  $Q_A^2 \equiv b_0 N_c \mu_A$  has now a slightly different meaning as compared to the fixed coupling case, but is still proportional to  $A^{1/3}$ . Here  $Q_A^2$  plays the role of saturation scale  $Q_s^2(A) = Q_A^2 \propto A^{1/3}$ . One can again separate the integral into the saturation and twist contributions, and all the qualitative properties of the Cronin peak are the same as in the fixed coupling case.

The main difference in the quantum evolution is the change of the energy and  $A$  dependences of the saturation scale (cf: eq. (8)): <sup>5,6,7</sup>

$$Q_s^2(A, y) \simeq \Lambda_{\text{QCD}}^2 \exp \left\{ \sqrt{2cby + \left( \ln Q_s^2(A) / \Lambda_{\text{QCD}}^2 \right)^2} \right\}, \quad (14)$$

where  $b = 12N_c / (11N_c - 2N_f)$  and  $c \simeq 4.88$  is the same number as in eq. (8). Namely, as the rapidity is increased, the saturation scale grows slower than in the fixed coupling case, and the nuclear  $A$  dependence becomes weaker and weaker and eventually disappears.<sup>7</sup> For example, due to this properties, the ratio goes to the universal value  $\mathcal{R}_{pA} \rightarrow 1/A^{1/3}$  at very high energy for a wide region of momenta.

## 5. Conclusion

We have presented an analytical understanding of the Cronin effect and high  $p_\perp$  suppression of the ratio  $\mathcal{R}_{pA}$  (2). All the properties observed in  $\mathcal{R}_{pA}$  are consistent with the nuclear modification factor measured by the Brahm's experiment. Therefore, we can naturally conclude that the CGC picture can be one of the most plausible explanations of the Brahm's data. This conclusion is now further confirmed by more quantitative analyses by other people.<sup>8</sup>

## References

1. I. Arsene, et al. (BRAHMS collaboration), nucl-ex/0403052 (ver.2).
2. D. Kharzeev, Y. Kovchegov, and K. Tuchin, Phys. Rev. **D68**, 094013 (2003).
3. J. Albacete, et al. Phys. Rev. Lett. **92**, 082001 (2004).
4. E. Iancu, K. Itakura and D. Triantafyllopoulos, Nucl. Phys. **A742**, 182 (2004).
5. E. Iancu, K. Itakura, and L. McLerran, Nucl. Phys. **A708**, 327 (2002).
6. A.H. Mueller and D. Triantafyllopoulos, Nucl. Phys. **B640**, 331 (2002).
7. A.H. Mueller, Nucl. Phys. **B724**, 223 (2003).
8. D. Kharzeev, Y. Kovchegov, and K. Tuchin, Phys. Lett. **B599**, 23 (2004), J. Jalilian-Marian, nucl-th/0402080.